HHS Public Access

Author manuscript

ACS Appl Mater Interfaces. Author manuscript; available in PMC 2021 November 08.

Published in final edited form as:

ACS Appl Mater Interfaces. 2020 November 25; 12(47): 52298–52306. doi:10.1021/acsami.0c12043.

Microbubbles Cloaked with Hydrogels as Activatable Ultrasound Contrast Agents

Mary W. N. Burns,

Department of Radiology, Translational Research in Ultrasound Theranostics (TRUST) Program and Biochemistry Graduate Program, University of Texas Southwestern Medical Center, Dallas, Texas 75390, United States

Robert F. Mattrey,

Department of Radiology, Translational Research in Ultrasound Theranostics (TRUST) Program, University of Texas Southwestern Medical Center, Dallas, Texas 75390, United States; Advanced Imaging Research Center, Dallas, Texas 75390, United States

Jacques Lux

Department of Radiology, Translational Research in Ultrasound Theranostics (TRUST) Program, Biomedical Engineering Graduate Program, and Organic Chemistry Graduate Program, University of Texas Southwestern Medical Center, Dallas, Texas 75390, United States

Abstract

Microbubbles (MBs) are optimal ultrasound contrast agents because their unique acoustic response allows for exquisite sensitivity *in vivo*. This unique response is derived from MBs' elasticity that allows them to oscillate differently from surrounding tissues. While the main use of MBs in the clinic is for cardiac and perfusion imaging, imparting MBs with bioresponsive properties would expand their use to detect pathophysiologic changes. This can be achieved by damping MBs' oscillations to silence their signal and rescuing it when they encounter the biomarker of interest to improve detection and specificity of diseases such as deep vein thrombosis (DVT). Here, we demonstrate that conjugating perfluorobutane-filled MBs with hyaluronic acid (HA) and cross-linking HA with biodegradable linkers eliminates harmonic signal because of increased MB stiffness and decreased oscillation. In this proof-of-concept study, we used a reversible pH-sensitive cross-linker to establish and validate this targeted and activatable

Corresponding Author: Jacques Lux − *Department of Radiology, Translational Research in Ultrasound Theranostics (TRUST) Program, Biomedical Engineering Graduate Program, and Organic Chemistry Graduate Program, University of Texas Southwestern Medical Center, Dallas, Texas 75390, United States*; Phone: (214) 648-5093; Jacques.Lux@UTSouthwestern.edu; Fax: (214) 648-5097.

Author Contributions

M.W.N.B., R.F.M., and J.L. designed the experiments. M.W.N.B. and J.L. performed the experiments and collected the data. M.W.N.B., R.F.M., and J.L. analyzed and interpreted the data. M.W.N.B. and J.L. performed the literature review. The manuscript was written through contributions of all authors. All authors have given approval to the final version of the manuscript.

ASSOCIATED CONTENT

Supporting Information

The Supporting Information is available free of charge at https://pubs.acs.org/doi/10.1021/acsami.0c12043.

Supplementary figures include A-HA-SH ^{1}H NMR spectrum and US images of HA-MBs and imine-crosslinked pH-MBs at neutral and acidic pH (PDF)

The authors declare no competing financial interest.

#Recipient of CPRIT Established Investigator Award (R.F.M.).

pH-sensitive MB (pH-MB) platform. Conjugation of HA to MBs and targeting of pH-MBs to CD44-positive cells were validated. Harmonic signal loss due to stiffening of pH-MBs' shell was confirmed using a clinical ultrasound scanner equipped with Cadence contrast pulse sequencing. pH-MBs imaged before and after acidification increased harmonic signal fivefold. Because the cleavage of the cross-linker we used is reversible, harmonic signal was silenced again when the acidic suspension was neutralized, confirming that harmonic signal is dependent on the cross-linked HA. The rate of rise and the magnitude of harmonic signal increase could be manipulated by varying the phospholipid composition and the number of HA cross-linkers, indicating that the platform can be tuned to the desired response needed. In this study, we established the feasibility of using targeted and activatable MBs and plan to apply this platform to aid in the diagnosis and management of patients with DVT and potentially other conditions.

Graphical Abstract

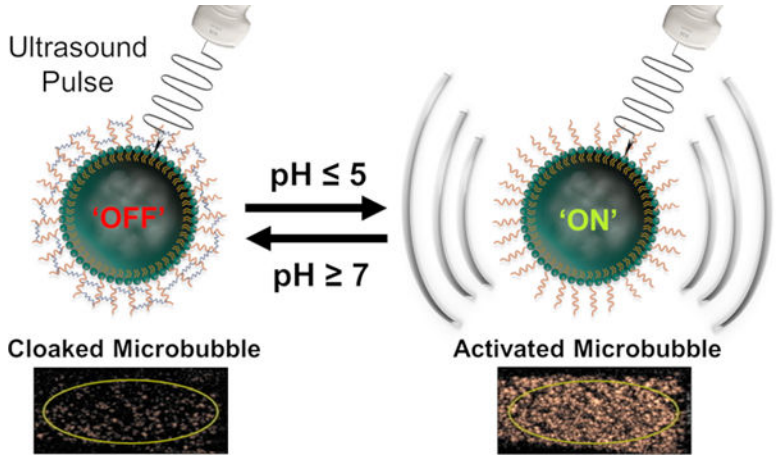

Keywords

ultrasound; activatable; microbubble; pH-sensitive; hydrogel; hyaluronic acid

INTRODUCTION

Microbubbles (MBs) are micron-sized particles with a gas core stabilized by a shell composed of either phospholipids, polymers, or proteins.[1,2] Owing to their elastic properties, MBs provide a much higher acoustic signal than surrounding tissues and exquisite imaging sensitivity, making them optimal contrast agents for ultrasound imaging at miniscule doses. While backscatter is the dominant component of the acoustic signal used in standard imaging, it is subtracted during contrast pulse sequencing (CPS) image generation to only show signals received at harmonic frequencies generated uniquely by the nonlinear oscillation of elastic MBs.[3] MBs derive their elasticity from their compressible gas core and soft shell that allow them to oscillate in response to an applied ultrasound pressure field. The nonlinear oscillations have been found, both theoretically and empirically, to depend on the mechanical properties of the shell that encapsulate and stabilize MBs.[4,5] Therefore, modulating MBs' oscillation in response to a specific biomarker would allow for an increase

in harmonic signals in response to different biological conditions.[1] More specifically, chemically induced switching between a stiff “off” state and an elastic “on” state would allow MBs to become detectable only when exposed to the biomarker of interest, such as pH,[6–8] reactive oxygen species,[8–10] hypoxia,[11,12] or enzymes.[13–15] Additionally, MBs can be targeted to receptors of interest by conjugating targeting ligands to their surface. Therefore, stiff-targeted MBs would become visible only if the biomarker is present at sites overexpressing the receptor, adding another layer of specificity.[16]

Currently, only two bioresponsive MB formulations have been proposed, and both are activated by thrombin and aimed to recognize active clotting in patients with deep vein thrombosis (DVT), a highly impactful clinical need.[17,18] Acute DVT is the active formation of blood clots in large veins of the body. Since fresh clots are loosely attached to the vessel wall, they can easily dislodge and cause a potentially fatal pulmonary embolus. As clots organize, they become firmly attached to the wall to cause potentially debilitating chronic venous disease rather than fatal embolism. Real-time ultra-sound with venous compression is the imaging modality of choice for the detection of DVT.[19,20] While fresh clots are invisible on ultrasound, they prevent the complete collapse of the vein during compression as indirect evidence of their presence. Once they begin to organize, they become visible on ultrasound. Since patients with previous DVT are at greater risk of developing new DVT, the presence of chronic clots prevents the recognition of superimposed active clotting, since the former prevents complete venous collapse on compression. Active clotting is treated aggressively with anticoagulants that can cause cerebral or internal hemorrhage in order to prevent fatal pulmonary embolism and decrease the severity of debilitating chronic venous disease. Since active clots cannot be excluded when chronic clots are present in symptomatic patients, they are treated empirically with anticoagulants, although the risk-to-benefit ratio is less clear since chronic clots do not respond to anticoagulation. Nakatsuka *et al.* used PAA/DNA anchors and thrombin-specific aptamer ligands as cross-linkers to stiffen the MB shell to dramatically reduce MBs’ harmonic signal. When the cross-linked MBs were exposed to high concentrations of thrombin, the aptamer cross-linkers were extracted, and the MBs’ harmonic signal was restored.[17] Since activated MBs remain visible until eliminated from the circulation unless rapidly activated on first pass through a clot, recirculation would fill the vessel with signal to decrease active clot recognition. Lux *et al.* used thrombin-cleavable peptides to increase the adhesion of elastic MBs in the presence of thrombin to recognize clots undergoing active thrombosis. Once peptides are cleaved, the MB surface becomes positively charged and adheres to the nearby negatively charged surfaces of endothelial cells, circulating cells that are carried away, or adjacent chronic clots downfield, decreasing specificity.

We developed targeted and bioresponsive MBs by attaching the biocompatible hyaluronic acid (HA) polymer to the phospholipid shell. Once HA is cross-linked, it becomes a hydrogel, stiffens the shell and silences harmonic signal. In this study, we used a reversible pH-sensitive cross-linker as a proof-of-concept to confirm and validate our platform (Figure 1), and we ultimately aim to use a thrombin-cleavable linker. Unlike the two previously reported platforms, our proposed MBs will be made to target and become trapped in clots. Once trapped, thrombin that is present in sufficient levels only in active clots will cleave the

cross-linker, allowing MBs to oscillate in the ultrasound field and turn on harmonic signal, highlighting only active clots and justifying treatment with risky anticoagulants.

To create a hydrogel scaffold around the MBs, we employed HA, a nonimmunogenic glycosaminoglycan composed of repeating disaccharide units of D-glucoronic acid and (1-β−3)-*N*-acetyl-D-glucosamine, which was oxidized and cross-linked with acid-labile hydrazone bonds. We chose HA due to its biocompatibility as well as its susceptibility to chemical modifications.[21] Furthermore, HA has previously been utilized to formulate hydrogels that deliver drugs in response to various biomarkers, such as redox conditions and matrix metal-loproteinases.[22–24] Although hydrazone-cross-linked HA hydrogels have been previously prepared,[25–27] this is the first report of hydrogel-coated MBs.

We oxidized thiolated HA (HA-SH) to obtain aldehyde-modified HA (A-HA) that we conjugated to maleimide-functionalized MBs (mal-MBs) via a thiol−ene coupling reaction and cross-linked A-HA with a 4-arm PEG-hydrazide forming hydrazone bonds and yielding pH-MBs. Importantly, the acid-triggered cleavage of hydrazone bonds is reversible; and the addition of base restores the bond after it has been cleaved by an acid. We demonstrated that pH-MBs target HeLa cells that are CD44-positive. Using a clinical ultrasound scanner with CPS, we observed a dramatic decrease in signal after cross-linking of the MBs. However, upon exposure to acid, hydrazone bonds contained in the shell of pH-MBs are cleaved, and elasticity of the pH-MBs is restored, resulting in a dramatic increase in CPS signal that is directly linked to harmonic signal generation. Additionally, we found that we can control pH-MB activation time and amplitude by changing parameters of our platform such as cross-linking density and MB shell composition.

Herein, we have developed a new tunable pH-sensitive ultrasound contrast agent and evaluated its response to acidic conditions *in vitro* as a proof-of-concept for a targeted and activatable MB platform. While we have used acidic pH as a biomarker of choice to demonstrate the feasibility of this approach, this activatable MB platform is versatile and could be modified to exploit other biomarkers such as enzymes, reactive oxygen species, and redox conditions. Changing the cross-linker, to an enzymatically degradable peptide for example, can directly change the functionality of the MB platform. In the future, we aim to apply this platform to diagnose DVT and potentially treat other diseases by taking advantage of an increase in MB oscillation to trigger drug/gene release.

RESULTS AND DISCUSSION

Synthesis and Characterization of A-HA-SH and Its Fluorescently Labeled Analogue.

In order to introduce aldehyde functionality to HA-SH (A-HA-SH), we oxidized HA-SH with sodium periodate according to the previously reported methods with slight modifications (Figure 3A) (see Experimental Section).[28] The degree of oxidation was 25%, as calculated using ^{1}H NMR by integrating the peaks of the aldehydes and comparing it to the integration for the peak of the methyl group on the *N*-acetylglucosamine monomer (Figure S1).[29,30] Thus, the resulting A-HA-SH bears thiols for easy conjugation to maleimide-terminated phospholipids on the MB shell and aldehyde moieties that can be reacted with cross-linkers containing terminal hydrazides and free amines.

Formulation of HA-MBs.

In the first step, perfluorobutane-filled (PFB-filled) MBs with a shell composed of 5 mol % of maleimide bearing phospholipids were formulated. Briefly, lipid films were solvated, and the mixture was sonicated with a PFB gas headspace to yield PEGylated maleimide-bearing MBs (mal-MBs). The size distribution and particle count were determined using a Coulter counter; and this formulation yielded MBs with a diameter of 2.70 ± 0.09 μm at a concentration of 2.82 ± 0.35 × 10^9 MB/mL in a volume of 0.80 mL. To confirm the successful conjugation of A-HA-SH to MBs, AlexaFluor 555-labeled aldehyde-modified HA-SH (AF555-A-HA-SH) was synthesized. The fluorescently labeled HA-SH was then added to maleimide-bearing DiD-labeled MBs. We observed colocalization of AF555 and DiD using fluorescence microscopy (Figure 2A) and flow cytometry (Figure 2B), confirming that AF555-HA was conjugated to MBs.

Once conjugation was validated using a fluorescent analogue, A-HA-SH was conjugated onto mal-MBs (Figure 3B) via a thiol−ene coupling. The resulting HA-MBs had a diameter of 3.02 ± 0.28 μm at a concentration of 3.38 ± 0.17 × 10^9 MB/mL in 0.60 mL. The decrease in MB count observed after HA conjugation can be attributed to a loss of MBs that are destroyed while being rotated end-over-end for at least 4 h. These reaction conditions can also lead to the coalescence of MBs increasing their mean diameter and decreasing their concentration.

Formulation of pH-MBs.

To obtain pH-MBs, the shell of HA-MBs was cross-linked with 4-arm PEG-hydrazide through the formation of acid-labile hydrazone bonds between the tetra-arm PEG-hydrazide and aldehyde functions on the A-HA backbone (Figure 3B),[27] effectively stiffening the MB shell with a hydrogel cloak. Following cross-linking, pH-MBs had a diameter of 3.37 ± 0.02 μm and a concentration of 1.20 ± 0.66 × 10^9 MB/mL in 0.6 mL. Similar to the conjugation step, the loss of MBs can be explained by end-over-end rotation that was performed for several hours to allow for the cross-linking reaction. The increase in mean diameter could be due to the coalescence of MBs or cross-linking between adjacent MBs.

In Vitro Targeting of pH-MBs to CD44-Positive HeLa Cells.

Targeting of pH-MBs to a human malignant cervical cancer cell line (HeLa), which has been shown to overexpress CD44,[31–33] was evaluated using an *in vitro* cell culture system. Fluorescently labeled pH-MBs, HA-MBs, and nontargeted precursor (mal-MBs) were incubated with HeLa cells, and targeting was assessed by fluorescence microscopy. For the negative, nontargeted control, we used mal-MBs, which are precursors to HA-MBs and pH-MBs and are not conjugated to any targeting ligand. The cells were incubated with MBs upside down, facilitating contact between buoyant MBs and adherent cells. The MB solution was aspirated from each well, and each well was washed three times with PFB-saturated PBS 1X. Targeting was assessed by bright field and fluorescence microscopy. As expected, HA-MBs targeted HeLa cells while mal-MBs did not (Figure 4). As with the HA-MBs, the pH-MBs also targeted HeLa cells, despite HA being chemically modified (Figure 3). This result demonstrates that HA retains its ability to target CD44 even after oxidation and cross-linking. This was expected since CD44 only binds to a short region of HA.[34] It is

worth noting that targeting of both HA-MBs and pH-MBs can be variable with regard to the amount of MBs/cell. This could be explained by a varying amount of CD44 receptors per cell as well as variable cell sizes. However, cells treated with nontargeted mal-MBs did not show any significant DiD signal (Figure 4), and the small number of MBs visible after the washing step is only due to nonspecific binding between mal-MBs and the cell surface. The CD44-targeting capability of pH-MBs demonstrates that hydrogel-cloaked MBs can be engineered to recognize specific receptors of interest in addition to being activatable.

REVERSIBLE ACID-TRIGGERED ACTIVATION OF PH-MBS

We assessed the effect of pH on the harmonic signal of pH-MBs *in vitro* using the setup shown in Figure 4C. Using a clinical ultrasound scanner equipped with CPS nonlinear harmonic imaging that displays the standard brightness-modulated (B-mode) image side-by-side with the MB-specific CPS image, we imaged 3×10^4 pH-MBs in a transfer pipette suspended in 3 mL PBS 1X at pH 7.4 (Figure 5A). While observing with real-time ultrasound imaging, the sample was acidified to pH 5 by adding HCl (Figure 5B). Regions of interest (ROIs) were drawn, and CPS signal intensity of pH-MBs was measured under neutral and acidic conditions. Upon addition of an acid, a fivefold increase in CPS signal was observed (Figure 5D). When noncross-linked HA-MBs were acidified, no change in harmonic signal was observed (Figure S2). pH-MB size distribution was assessed before and after acidification, and no significant change was observed (2.05 ± 0.05 at pH 7.4 vs 1.84 ± 0.1 μm at pH 5), indicating that the change in harmonic signal after acidification is solely due to increased elasticity.

As the acid-mediated cleavage of hydrazone bonds is reversible, we confirmed the reversibility of this platform by adding NaOH to the sample to neutralize pH. We observed that the CPS signal intensity returned to the preacidification baseline, and reacidification regenerated the lost CPS signal and so on for several acidification/neutralization cycles. We measured the CPS signal intensity before and after each cycle, and observed that peak intensity slightly decreased after each cycle (Figure 5E), due in part to MB destabilization by NaOH, progressive MB dilution, and more important MB destruction by ultrasound due to the over 30 min continual real-time imaging. This phenomenon will not occur *in vivo* since ultrasound study time is relatively short, and MBs will not be exposed to a strong base to destabilize them. Although reversible activation around pH 5 is not biologically relevant, it provides an internal control of the system and a robust proof-of-concept that harmonic signal generation is due to the cross-linked HA. This approach also provided us critical insight to optimize cross-linking parameters and shell composition to both increase signal rise time and amplitude. The results from both the targeting experiment and *in vitro* activation demonstrated that the MBs cloaked in cross-linked hydrogels can be both targeted and activated by a biomarker of interest.

In addition to the formulation of pH-MBs using 4-arm PEG hydrazide, we also used a 4-arm PEG-amine cross-linker, which reacts with the aldehyde groups on A-HA-SH to form imine linkages. Imine linkages are also acid labile and have been used to develop pH-sensitive materials by other groups.[35,36] pH-MB cross-linked with 4-arm PEG-amine exhibited similar ultra-sound behavior upon acidification (Figure S3). This suggests that this

HA cross-linking platform is versatile and can be configured using other clinically relevant biomarkers, such as thrombin-cleavable peptides.

Effect of Cross-Linking Parameters on pH-MB Activation.

To maximize the ultrasound signal enhancement and shorten the activation time, various formulation parameters were screened, including maleimide mol % on the MB shell, equivalents of cross-linker, and cross-linker lengths. We observed that the greater the cross-linker equivalents, the lesser the difference in CPS signal between the “off” and “on” states and the longer the time to reach peak signal (Figure 6). Since rapid increase in signal is preferred in biologic systems, the cross-linker equivalents should be the lowest needed to maintain MB stiffness in order to minimize harmonic signal at neutral pH.

The basis for this observation is that the more the cross-linkers and the stiffer the cloak, the lower the signal at neutral pH and the longer it will take to cleave all hydrazone linkers to restore shell elasticity. As MB oscillation is restored, MB destruction by ultrasound increases to further decrease signal. Of interest is that harmonic silencing occurred following the inclusion of a small amount of cross-linkers.

The length of the acyl chain of phospholipids used in the pH-MB shells also contributed to peak signal and time to reach peak enhancement. The most pronounced difference was between DSPC-based (18-C chain length) and DPPC-based (16-C chain length) shells. The 18-C lipid decreased peak enhancement from 5-to 1.8-fold and increased the time to peak from 2 to 16 min, likely due to the more homogeneous distribution of DSPE-PEG on the DPPC-based MB shell compared to DSPC,[37,38] which we believe contributes to better cloaking of MBs and a more rapid degradation when the cross-linkers are disrupted. Replacing the DSPE-PEG2k-mal with DPPE-PEG2k-mal of DSPC pH-MBs did not improve their performance. This is likely because the 16-C acyl chains of DPPE-PEG2k-HA participate in fewer intermolecular inter-actions than its 18-C counterpart, allowing HA to move more freely over the MB surface, which decreases the change in elasticity after acidification and therefore harmonic signal generation.

These results show that the activation time and signal enhancement of pH-MBs can be tuned by manipulating the phospholipid composition of the MB shell as well as the amount of cross-linker incorporated in the degradable hydrogel cloak.

CONCLUSIONS

Ultrasound is a portable, accessible, and safe imaging modality, and the development of biocompatible and activatable ultrasound contrast agents is critical for expanding its clinical utility. Though ultrasound is exquisitely sensitive to MBs and has been used to detect targeted MBs, bioresponsive MBs with an “on” and “off” signal switch are currently limited. Biocompatible “smart” MBs would allow for a more accurate and precise diagnosis of diseases that already rely on ultrasound scanners for detection. In this study, we showed that cloaking MBs with a biodegradable hydrogel yields CD44-targeted MBs that reversibly increase their signal fivefold in response to acidic pH, a biomarker of tumor microenvironments. The reversible nature of the covalent bonds between HA and the cross-

linkers resulted in a reversed CPS signal, confirming that the change in CPS signal is due to the presence or absence of the cross-links that impacted the elasticity of pH-sensitive MBs. These results provide a robust proof-of-concept for this targeted and activatable platform. Given the facile preparation of MBs cloaked with HA hydrogel, MBs sensitive to other environmental conditions can be made by altering the cross-linkers' reactivity. This is the first report of hydrogel-cloaked MBs, as well as activatable MBs that can easily be engineered to be responsive to various biomarkers of disease. We are planning to use this platform to develop thrombin-sensitive MBs for the detection of acute DVT. More broadly, we plan to use this smart MB platform and take advantage of increased MB oscillation to not only aid in detection but also increase drug release or gene delivery to treat a variety of diseases, including cancer.

EXPERIMENTAL SECTION

Materials and Methods.

Lipids were purchased from Avanti Polar Lipids, Inc. (AL, USA) and NanoCS. (MA, U.S.A.). Perfluorobutane was purchased from FluoroMed LP (Round Rock, TX). DiD was purchased from Thermo Fisher Scientific (IL, USA). For regular MBs, Definity (perflutren lipid microsphere) was purchased from Lantheus Medical Imaging, Inc. (MA, USA). Thiolated hyaluronic acid (10 kDa) was purchased from Creative PEGWorks Inc. (NC, USA). Other chemicals were purchased from Sigma-Aldrich (MO, USA) and Thermo Fisher Scientific (MA, USA) and used without further purification. Microbubble sizing and counting were performed using a Multisizer 4 Coulter Counter system (Beckman Coulter Inc., CA, USA). Microbubbles were sonicated with a tip sonicator (Branson Ultrasonics, TX, U.S.A.). Flow cytometry experiments were performed using a multiwavelength BD Accuri C6 flow cytometer (BD Biosciences, San Jose, CA). Microscopy experiments were performed using an Axio A1 upright fluorescence microscope (Carl Zeiss AG, Germany) equipped with a mercury lamp and a variety of filter sets (DAPI, FITC, TRITC, and Cy5). Ultrasound imaging experiments were performed at 7 MHz using a clinical Siemens Acuson Sequoia 512 ultrasound system (Siemens Healthcare, Mountain View, CA) equipped with a 15 L8 transducer.

Formulation and Characterization of Maleimide-Bearing Microbubbles (Mal-MBs).

Perfluorobutane (C_4H_{10}, PFB)-filled MBs with a phospholipid shell containing 1,2-dipalmitoyl-*sn*-glycero-3-phosphocholine (DPPC) (Avanti Polar Lipids), 1,2-distearoyl-*sn*-glycero-3-phosphoethanolamine-(polyethylene glycol)-2000 (DSPE-PEG2k) (NanoCS), and 1,2-distearoyl-*sn*-glycero-3-phosphoethanolamine-*N*[maleimide(polyethylene glycol)-2000 (DSPE-PEG2k-Mal) (NanoCS) in a 90:5:5 molar ratio were formulated. Briefly, lipid films were solvated in a mixture of PBS 1X/propylene glycol/glycerol (8:1:1 v/v/v, 10 mL), heated in a heating block until the solution reached 65 °C, and then bath sonicated at 70 °C until the solution was clear. PFB gas was then introduced into the headspace, and the lipid solution was sonicated for 5 s with a tip sonicator (Branson). The vial was then cooled down in an ice bath for 5 min. Foam was removed via syringe transfer, and the MBs were washed by slow centrifugation (300 g, 3 min, 3 times) with PBS 1X, pH 6.5, and 1 mM EDTA (4 mL) to

yield PEGylated MBs with maleimide functionality. The MBs were then sized and counted using a Beckman Multisizer 4.

Synthesis and Characterization of Aldehyde-Modified Thiolated HA (A-HA-SH).

A-HA-SH was synthesized according to the previously reported procedure with slight modifications.[28] Briefly, 100.0 mg HA-SH (10 kDa, 0.01 mmol, Creative PEGWorks) was dissolved in nanopure H_2O (10 mL, milliQ, Millipore Sigma) at a concentration of 10 mg/mL. An aqueous solution of sodium periodate (0.5 M, 1.06 mL, Sigma-Aldrich) was added, and the reaction was stirred for 4 h at room temperature in the dark. After this time, ethylene glycol (1 mL, Sigma-Aldrich) was added to inactivate any unreacted periodate. The reaction was stirred for another hour at room temperature, and the resulting reaction mixture was dialyzed exhaustively against H_2O and lyophilized. The oxidation of A-HA-SH was confirmed by ^{1}H NMR. ^{1}H NMR (400 MHz, D_2O, δ): 4.85 (s, 1H), 4.95 (s, 1H), and 5.05 (s, 1H) ppm.

Preparation and Characterization of Aldehyde-Modified Hyaluronic Acid MBs (A-HA-MBs).

A-HA-MBs were obtained by conjugating A-HA-SH to the 90:5:5 mal-MBs through a thiol−ene coupling reaction. Mal-MBs were diluted in PBS 1X (pH 6.5, 1 mM EDTA) to a concentration of 3.5×10^9, and 100 μL of 10 mg/mL A-HA-SH solution was added (5 eq.), and the mixture was rotated end-over-end (4 h, room temperature, pH 6.5, 1 mM EDTA). The resulting A-HA-MBs were washed by slow centrifugation (300 g, 3 min, 3 times) with PBS 1X (pH 7.4) and characterized with a Beckman Multisizer 4.

Synthesis of AlexaFluor 555-Labeled HA-SH (AF555-HA-SH).

HA-SH was fluorescently labeled with AlexaFluor 555 using 1-ethyl-3-(3-dimethylaminopropyl)carbodiimide (EDC) and *N*-hydroxysuccinimide (NHS) as coupling agents. Briefly, HA-SH (10 kDa, 25 mg, 0.0075 mmol, CreativePEGWorks) was first dissolved in nanopure H_2O (2.5 mL, milliQ, Millipore Sigma). Then, solutions of EDC (0.0083 mmol) and NHS (0.0083 mmol) were added to the HA-SH solution. Next, a 1 mg/mL solution of AF-555 hydrazide was added (0.000125 mmol, Thermo Fisher). The reaction was stirred in the dark overnight, and the reaction mixture was dialyzed exhaustively against H_2O and lyophilized.

Preparation and Characterization of AF555-HA-MBs.

AF555-HA-MBs were obtained by conjugating AF555-HA to DiD-labeled MBs through a thiol−ene coupling reaction with a procedure identical to that of the A-HA-SH MBs. The resulting AF555-HA-MBs were washed by slow centrifugation as (300 g, 3 min, 3 times) with PBS 1X (pH 7.4) and characterized using a Beckman Multisizer 4.

Preparation and Characterization of Acid-Sensitive Cross-Linked MBs (pH-MBs).

PEG2k-hydrazide (4-arm, Creative PEG-Works) was used to cross-link the A-HA conjugated to the surface of the MBs. The previously formulated A-HA-MBs (0.2 mL) were diluted in PBS 1X (pH 7.4) to a concentration of 1×10^9 MB/mL, 0.20 μL of 10 mg/mL 4-arm PEG2k-hydrazide (0.1 eq.) was added, and the mixture was rotated end-over-end for

4 h at room temperature. The resulting pH-MBs were then stored at 4 °C and characterized using a Beckman Multisizer 4. pH-MBs were stored at 4°C in an aqueous solution and used within one week of formulation.

In Vitro Assessment of pH-MB Targeting to CD44+ HeLa Cells.

pH-MBs, HA-MBs, and nontargeted mal-MBs were formulated as described above and labeled with DiD to evaluate targeting by fluorescence microscopy. Briefly, HeLa cells were plated in a 12-well plate at 400 000 cells/well. When the cells reached 75−90% confluence, pH-MBs, HA-MBs (positive control), and nontargeted MBs (negative control) suspended in PFB-saturated media were all added to separate wells. For the negative, nontargeted control, we used mal-MBs, which are precursors to HA-MBs and pH-MBs and are not conjugated to any targeting ligand. For each formulation, a ratio of 3 MBs/cell was used. The cells were incubated with MBs upside down, facilitating contact between buoyant MBs and adherent cells. The MB solution was aspirated from each well, and each well was washed three times with PFB-saturated PBS 1X. Targeting was assessed by bright field and fluorescence microscopy. Experiments were performed in triplicate for each condition.

In Vitro Ultrasound Imaging of pH-MBs in Neutral or Acidic Conditions.

A suspension of pH-MBs (1×10^4 MBs) in PBS 1X (pH 7.4, 3 mL) was placed at 37 °C in a transfer plastic pipette bulb inside a tissue-mimicking sample holder composed of 1% agar and 0.5% corn starch. To image the pH-MBs at pH 5, 0.1 M HCl (70 μL) was added to acidify the suspension. The sample was imaged using a clinical ultrasound scanner (Siemens Acuson Sequoia 512) equipped with a 15 L8 imaging transducer (Mountain View, CA). An MB-sensitive contrast pulsing sequence (CPS) imaging mode was used and displayed side by side with a brightness-modulated (B-mode) image for bulb visualization and placement as well as for an internal control. Regarding the CPS imaging mode, the system utilizes a multipulse technique with phase and amplitude modulation to subtract nonMB signal in real-time, resulting in a MB-only CPS image. The acoustic pressure was set at a mechanical index (MI) of 0.07 and imaged at 7 MHz. The MI is linearly related to peak negative pressure and inversely related to the square root of the transmitted frequency. Cine loops of real-time imaging were recorded before and after the addition of acid until the pH-MBs reached their maximum signal intensity. We used ImageJ to quantify the ultrasound signal of pH-MBs before and after acidifying the solution. Ellipsoidal regions-of-interest (ROIs) were drawn on the B-mode and the CPS ultrasound images, and the mean image intensity (a.u.) was measured. All imaging experiments were done in triplicate. Statistically significant differences between groups were assessed by performing student’s t-tests using Welch’s correction.

Supplementary Material

Refer to Web version on PubMed Central for supplementary material.

ACKNOWLEDGMENTS

The authors acknowledge Siemens Medical Solutions USA. Inc. for the ultrasound equipment loan and for the implementation of the MRSQ software on the ultrasound scanner. J.L. acknowledges Erin Moore (Creatives Services, Department of Radiology, University of Texas Southwestern Medical Center) for the cover art.

Funding

This work was supported by the Cancer Prevention and Research Institute of Texas (RR150010 and RP190233). MWNB was supported in part by NIH T32GM127216. The content is solely the responsibility of the authors and does not necessarily represent the official views of the NIH.

ABBREVIATIONS

DPPC	1,2-dipalmitoyl-*sn*-glycero-3-phosphocholine DSPE-PEG(2000)-mal, 1,2-distearoyl-*sn*-glycero-3-phosphoethanolamine-*N*-[maleimide(polyethylene glycol)-2000] DSPE-PEG(2000), 1,2-distearoyl-*sn*-glycero-3-phosphoethanolamine-*N*-[amino(polyethylene glycol)-2000]
HA	hyaluronic acid
HA-SH	thiolated hyaluronic acid
A-HA-SH	aldehyde-modified hyaluronic acid
pH-MBs	pH-sensitive cross-linked MBs
EDTA	ethylenediaminetetraacetic acid
EDC	1-ethyl-3-(3-dimethylaminopropyl)carbodiimide
NHS	*N*-hydroxysuccinimide
FITC	fluorescein isothiocyanate
MB	microbubble
NMR	nuclear magnetic resonance
PFB	perfluorobutane
ROS	reactive oxygen species
ROI	region of interest

REFERENCES

(1). Goodwin AP; Nakatsuka MA; Mattrey RF Stimulus−Responsive Ultrasound Contrast Agents for Clinical Imaging: Motivations, Demonstrations, and Future Directions. WIREs Nanomed. Nanobiotechnol 2015, 7, 111–123.

(2). Stride E; Segers T; Lajoinie G; Cherkaoui S; Bettinger T; Versluis M; Borden M Microbubble Agents: New Directions. Ultrasound Med. Biol 2020, 46, 1326–1343. [PubMed: 32169397]

(3). Sboros V Response of Contrast Agents to Ultrasound. Adv. Drug Delivery Rev 2008, 60, 1117–1136.

(4). Hoff L; Sontum PC; Hovem JM Oscillations of Polymeric Microbubbles: Effect of the Encapsulating Shell. J. Acoust. Soc. Am 2000, 107, 2272–2280. [PubMed: 10790053]

(5). Church CC The Effects of an Elastic Solid Surface Layer on the Radial Pulsations of Gas Bubbles. J. Acoust. Soc. Am 1995, 97, 1510–1521.

(6). Webb BA; Chimenti M; Jacobson MP; Barber DL Dysregulated Ph: A Perfect Storm for Cancer Progression. Nat. Rev. Cancer 2011, 11, 671–677. [PubMed: 21833026]

(7). Martínez-Zaguilán R; Seftor EA; Seftor REB; Chu Y-W; Gillies RJ; Hendrix MJC Acidic Ph Enhances the Invasive Behavior of Human Melanoma Cells. Clin. Exp. Metastasis 1996, 14, 176–186. [PubMed: 8605731]

(8). Viger ML; Collet G; Lux J; Nguyen Huu VA; Guma M; Foucault-Collet A; Olejniczak J; Joshi-Barr S; Firestein GS; Almutairi A Distinct on/Off Fluorescence Signals from Dual-Responsive Activatable Nanoprobes Allows Detection of Inflammation with Improved Contrast. Biomaterials 2017, 133, 119–131. [PubMed: 28433935]

(9). Reuter S; Gupta SC; Chaturvedi MM; Aggarwal BB Oxidative Stress, Inflammation, and Cancer: How Are They Linked. Free Radical Biol. Med 2010, 49, 1603–1616. [PubMed: 20840865]

(10). Hecht F; Pessoa CF; Gentile LB; Rosenthal D; Carvalho DP; Fortunato RS The Role of Oxidative Stress on Breast Cancer Development and Therapy. Tumor Biol 2016, 37, 4281–4291.

(11). Okuda K; Okabe Y; Kadonosono T; Ueno T; Youssif BGM; Kizaka-Kondoh S; Nagasawa H 2-Nitroimidazole-Tricarbocyanine Conjugate as a near-Infrared Fluorescent Probe for in Vivo Imaging of Tumor Hypoxia. Bioconjugate Chem 2012, 23, 324–329.

(12). Krohn KA; Link JM; Mason RP Molecular Imaging of Hypoxia. J. Nucl. Med 2008, 49, 129S–148S. [PubMed: 18523070]

(13). Overall CM; Kleifeld O Validating Matrix Metalloproteinases as Drug Targets and Anti-Targets for Cancer Therapy. Nat. Rev. Cancer 2006, 6, 227–239. [PubMed: 16498445]

(14). Xu D; McKee CM; Cao Y; Ding Y; Kessler BM; Muschel RJ Matrix Metalloproteinase-9 Regulates Tumor Cell Invasion through Cleavage of Protease Nexin-1. Cancer Res 2010, 70, 6988–6998. [PubMed: 20736374]

(15). Coughlin SR Thrombin Signalling and Protease-Activated Receptors. Nature 2000, 407, 258–264. [PubMed: 11001069]

(16). Klibanov AL Microbubble Contrast Agents: Targeted Ultrasound Imaging and Ultrasound-Assisted Drug-Delivery Applications. Invest. Radiol 2006, 41, 354–362. [PubMed: 16481920]

(17). Nakatsuka MA; Mattrey RF; Esener SC; Cha JN; Goodwin AP Aptamer-Crosslinked Microbubbles: Smart Contrast Agents for Thrombin-Activated Ultrasound Imaging. Adv. Mater 2012, 24, 6010–6016. [PubMed: 22941789]

(18). Lux J; Vezeridis AM; Hoyt K; Adams SR; Armstrong AM; Sirsi SR; Mattrey RF Thrombin-Activatable Microbubbles as Potential Ultrasound Contrast Agents for the Detection of Acute Thrombosis. ACS Appl. Mater. Interfaces 2017, 9, 37587–37596. [PubMed: 28994575]

(19). Coley BD; Trambert MA; Mattrey RF Perfluorocarbon-Enhanced Sonography: Value in Detecting Acute Venous Thrombosis in Rabbits. AJR Am. J. Roentgenol 1994, 163, 961–964. [PubMed: 8092043]

(20). Heng Tan C; Bedi D; Vikram R Sonography of Thrombosis of the Deep Veins of the Extremities: Clinical Perspectives and Imaging Review. J. Clin. Ultrasound 2012, 40, 31–43. [PubMed: 22105376]

(21). Naor D; Sionov RV; Ish-Shalom D Cd44: Structure, Function, and Association with the Malignant Process. Adv. Cancer Res 1997, 71, 241–319. [PubMed: 9111868]

(22). Yang C; Li C; Zhang P; Wu W; Jiang X Redox Responsive Hyaluronic Acid Nanogels for Treating Rhamm (Cd168) over-Expressive Cancer Both Primary and Metastatic Tumors. Theranostics 2017, 7, 1719–1734. [PubMed: 28529647]

(23). Yang Y; Zhu H; Wang J; Fang Q; Peng Z Enzymatically Disulfide-Crosslinked Chitosan/Hyaluronic Acid Layer-by-Layer Self-Assembled Microcapsules for Redox-Responsive Controlled Release of Protein. ACS Appl. Mater. Interfaces 2018, 10, 33493–33506. [PubMed: 30203959]

(24). Purcell BP; Lobb D; Charati MB; Dorsey SM; Wade RJ; Zellars KN; Doviak H; Pettaway S; Logdon CB; Shuman JA; Freels PD; Gorman JH III; Gorman RC; Spinale FG; Burdick JA

Injectable and Bioresponsive Hydrogels for on-Demand Matrix Metalloproteinase Inhibition. Nat. Mater 2014, 13, 653–661. [PubMed: 24681647]

(25). Fu C; Li H; Li N; Miao X; Xie M; Du W; Zhang L-M Conjugating an Anticancer Drug onto Thiolated Hyaluronic Acid by Acid Liable Hydrazone Linkage for Its Gelation and Dual Stimuli-Response Release. Carbohydr. Polym 2015, 128, 163–170. [PubMed: 26005152]

(26). Wang LL; Chung JJ; Li EC; Uman S; Atluri P; Burdick JA Injectable and Protease-Degradable Hydrogel for Sirna Sequestration and Triggered Delivery to the Heart. J. Controlled Release 2018, 285, 152–161.

(27). Šedová P; Buffa R; Šilhár P; Kovářová L; Vágnerová H; Bednařík J; Basarabová I; Hejlová L; Ščĭgalková I; Šimek M; Velebný V The Effect of Hydrazide Linkers on Hyaluronan Hydrazone Hydrogels. Carbohydr. Polym 2019, 216, 63–71. [PubMed: 31047083]

(28). Li L; Wang N; Jin X; Deng R; Nie S; Sun L; Wu Q; Wei Y; Gong C Biodegradable and Injectable in Situ Cross-Linking Chitosan-Hyaluronic Acid Based Hydrogels for Postoperative Adhesion Prevention. Biomaterials 2014, 35, 3903–3917. [PubMed: 24507411]

(29). Huang Y; Zhang X; Wu A; Xu H An Injectable Nano-Hydroxyapatite (N-Ha)/Glycol Chitosan (G-Cs)/Hyaluronic Acid (Hya) Composite Hydrogel for Bone Tissue Engineering. RSC Adv 2016, 6, 33529–33536.

(30). Li X; Kong X; Zhang Z; Nan K; Li L; Wang X; Chen H Cytotoxicity and Biocompatibility Evaluation of N,O-Carboxymethyl Chitosan/Oxidized Alginate Hydrogel for Drug Delivery Application. Int. J. Biol. Macromol 2012, 50, 1299–1305. [PubMed: 22465755]

(31). Bruno S; Fabbi M; Tiso M; Santamaria B; Ghiotto F; Saverino D; Tenca C; Zarcone D; Ferrini S; Ciccone E; Grossi CE Cell Activation Via Cd44 Occurs in Advanced Stages of Squamous Cell Carcinogenesis. Carcinogenesis 2000, 21, 893–900. [PubMed: 10783309]

(32). Uhlén M; Fagerberg L; Hallström BM; Lindskog C; Oksvold P; Mardinoglu A; Sivertsson Å; Kampf C; Sjöstedt E; Asplund A; Olsson I; Edlund K; Lundberg E; Navani S; Szigyarto CA-K; Odeberg J; Djureinovic D; Takanen JO; Hober S; Alm T; Edqvist P-H; Berling H; Tegel H; Mulder J; Rockberg J; Nilsson P; Schwenk JM; Hamsten M; von Feilitzen K; Forsberg M; Persson L; Johansson F; Zwahlen M; von Heijne G; Nielsen J; Pontén F Tissue-Based Map of the Human Proteome. Science 2015, 347, 1260419. [PubMed: 25613900]

(33). Wang K; Zeng J; Luo L; Yang J; Chen J; Li B; Shen K Identification of a Cancer Stem Cell-Like Side Population in the Hela Human Cervical Carcinoma Cell Line. Oncol. Lett 2013, 6, 1673–1680. [PubMed: 24260061]

(34). Banerji S; Wright AJ; Noble M; Mahoney DJ; Campbell ID; Day AJ; Jackson DG Structures of the Cd44−Hyaluronan Complex Provide Insight into a Fundamental Carbohydrate-Protein Interaction. Nat. Struct. Mol. Biol 2007, 14, 234–239. [PubMed: 17293874]

(35). Su H; Zhang W; Wu Y; Han X; Liu G; Jia Q; Shan S Schiff Base-Containing Dextran Nanogel as pH-Sensitive Drug Delivery System of Doxorubicin: Synthesis and Characterization. J. Biomater. Appl 2018, 33, 170–181. [PubMed: 29940809]

(36). Zhang Z; He C; Chen X Hydrogels Based on Ph-Responsive Reversible Carbon−Nitrogen Double-Bond Linkages for Biomedical Applications. Mater. Chem. Front 2018, 2, 1765–1778.

(37). Kooiman K; Kokhuis TJA; van Rooij T; Skachkov I; Nigg A; Bosch JG; van der Steen AFW; van Cappellen WA; de Jong N DSPC or DPPC as Main Shell Component Influences Ligand Distribution and Binding Area of Lipid-Coated Targeted Microbubbles. Eur. J. Lipid Sci. Technol 2014, 116, 1217–1227.

(38). Langeveld SAG; Schwieger C; Beekers I; Blaffert J; van Rooij T; Blume A; Kooiman K Ligand Distribution and Lipid Phase Behavior in Phospholipid-Coated Microbubbles and Mono-layers. Langmuir 2020, 36, 3221–3233. [PubMed: 32109064]

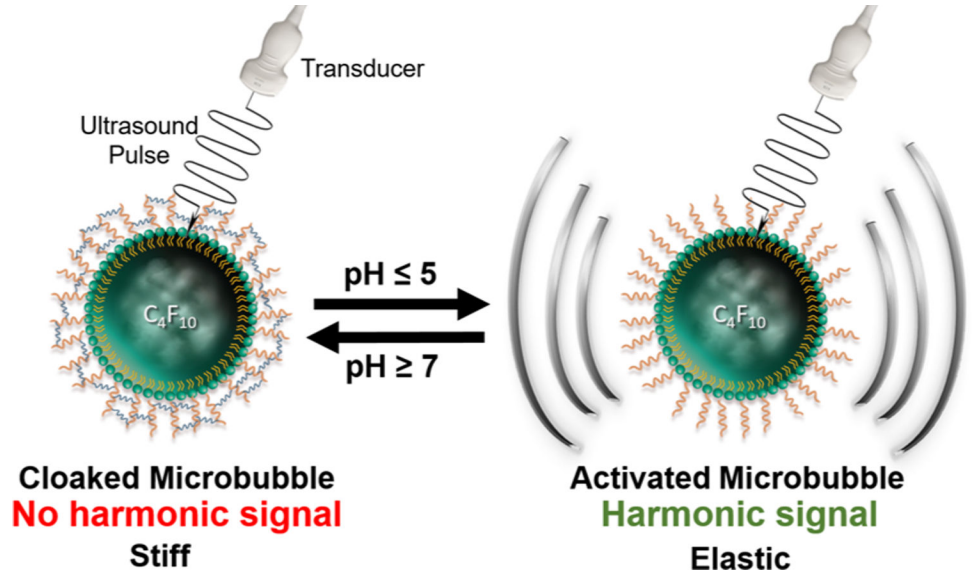

Figure 1.
Schematic representation of reversible activation of pH-sensitive microbubbles.

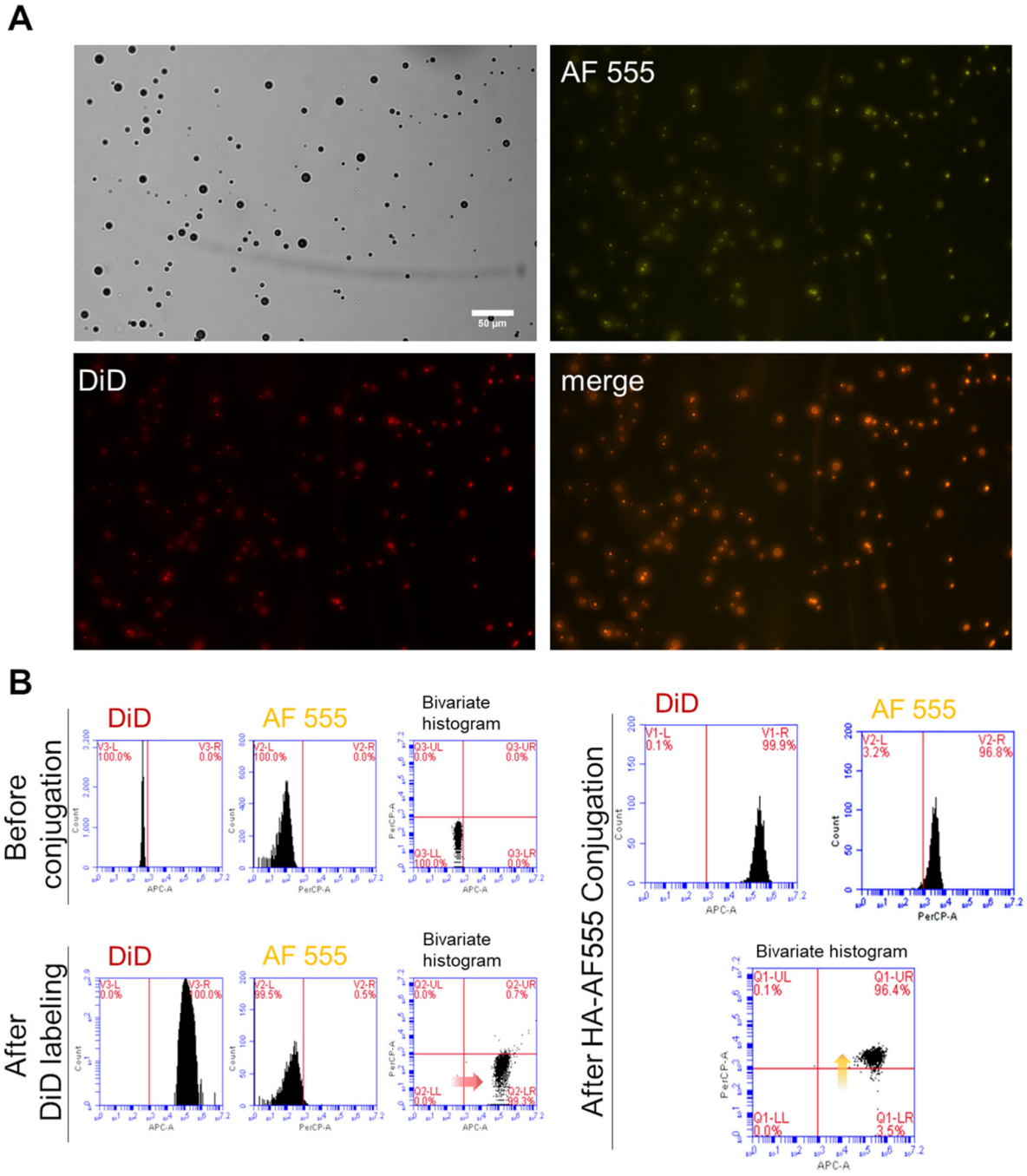

Figure 2.

Validation of MB conjugation with fluorescent analogue of HA. (A) Bright field and fluorescence microscopy images of DiD-labeled AF555-HA-MBs. Scale bar is 50 μm. (B) Characterization of AF555-HA-MBs by flow cytometry before and after DiD labeling and AF555-A-HA-SH conjugation.

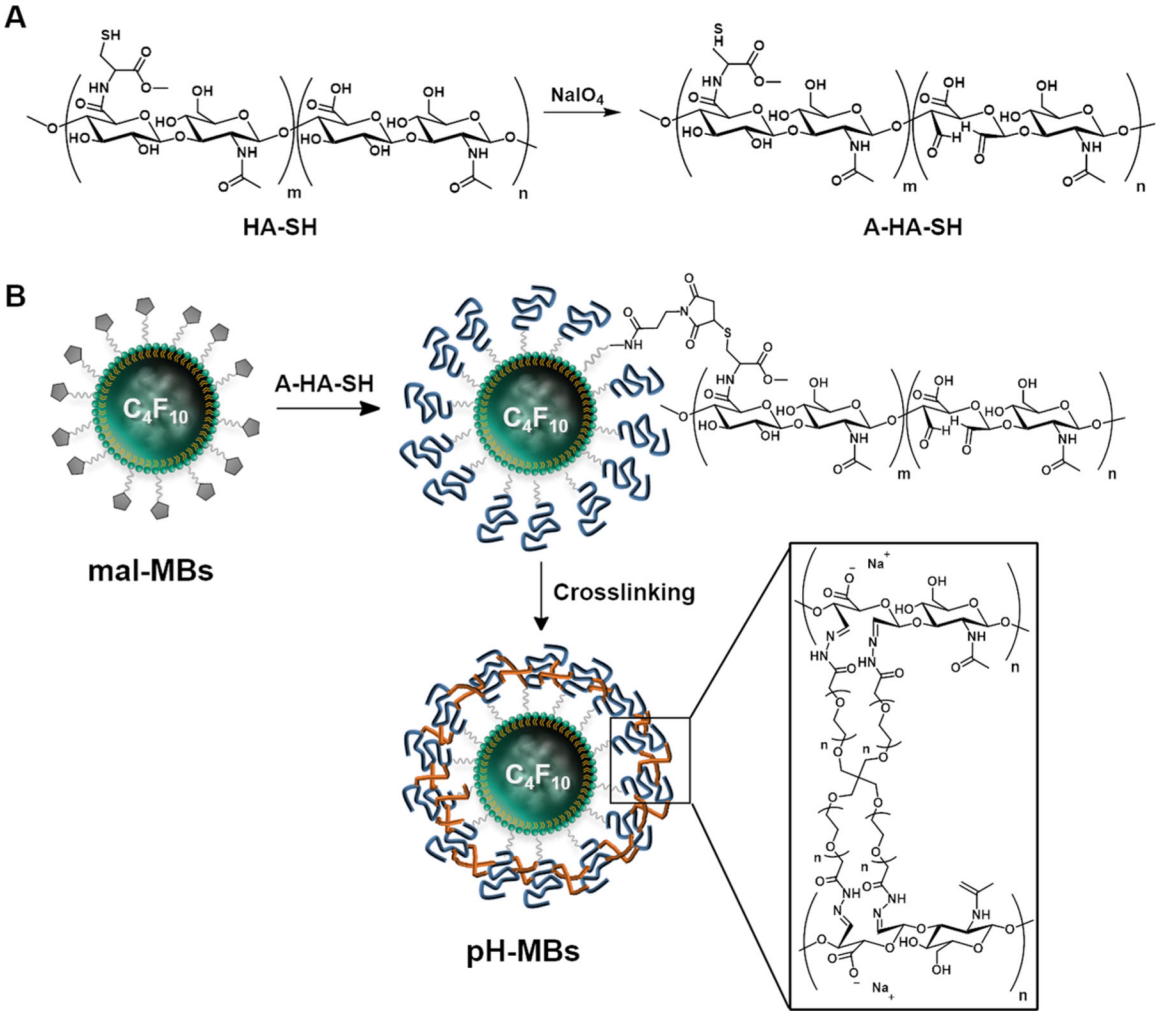

Figure 3.

Formulation of pH-MBs. (A) Synthesis of A-HA-SH. (B) Schematic representation of conjugation of A-HA-SH to mal-MBs and subsequent cross-linking of A-HA with pH-sensitive cross-linker to yield pH-MBs.

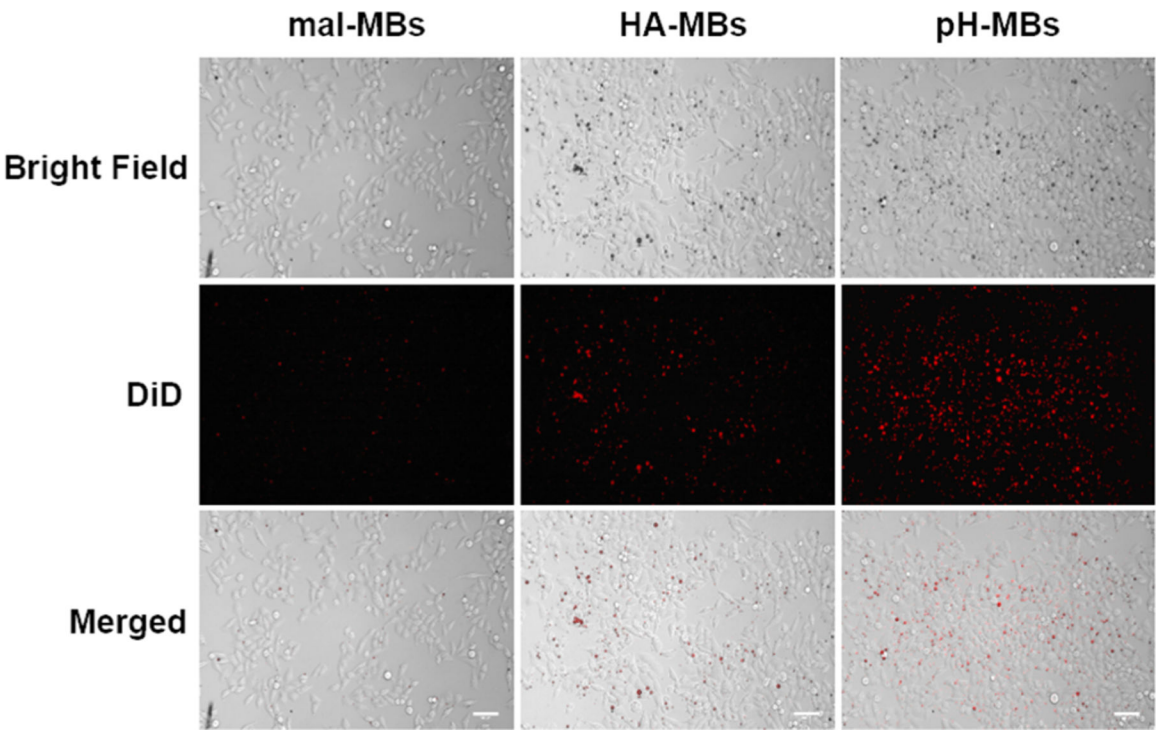

Figure 4.

Representative bright field and fluorescence microscopy pictures of HeLa cells treated with DiD-labeled pH-MBs, HA-MBs, and mal-MBs. Scale bar is 100 μm.

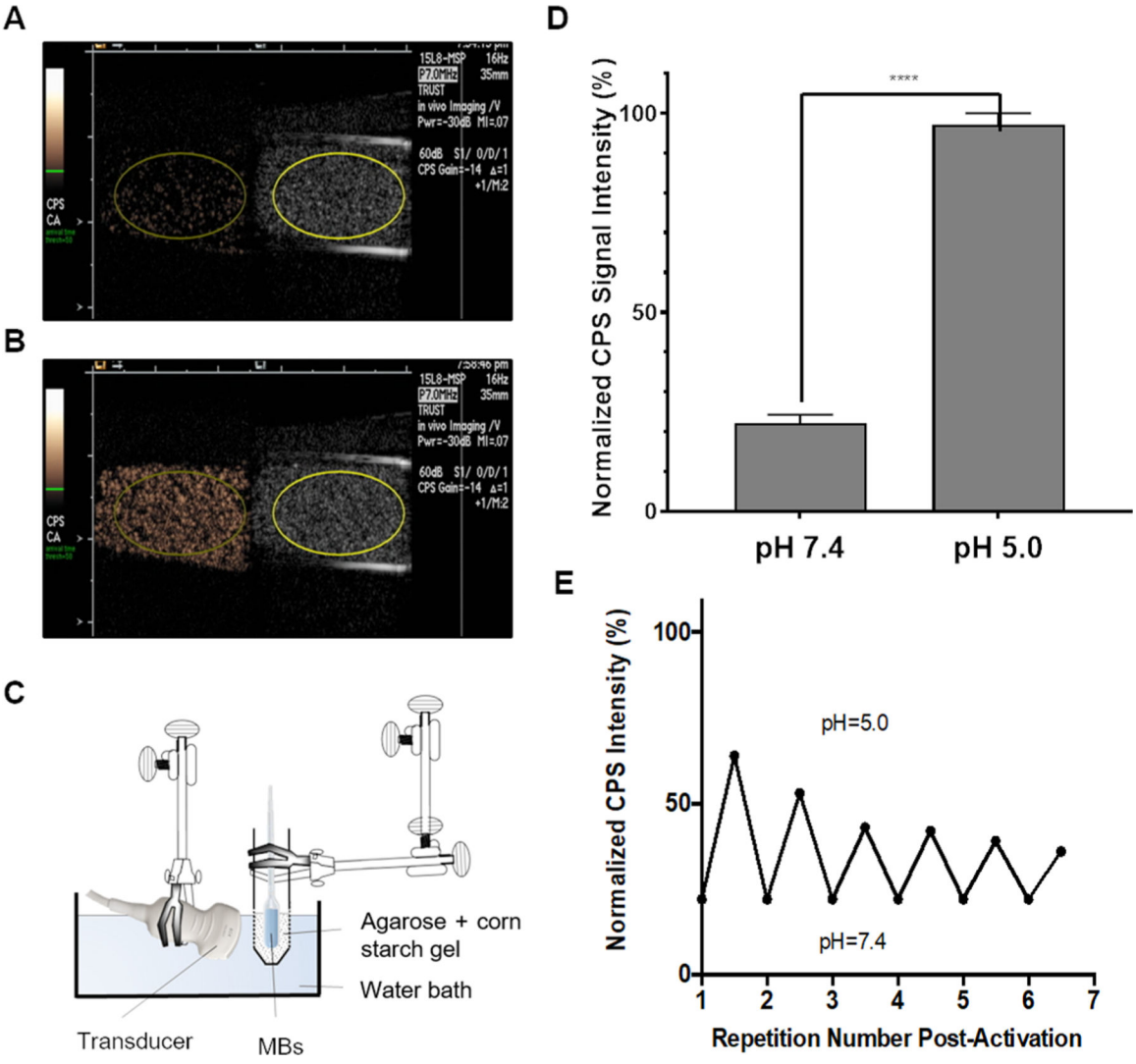

Figure 5.

pH-MBs imaged with CPS (left) and B-Mode (right) (A) at pH 7.4 and (B) at pH 5 using the *in vitro* setup shown in (C). (D) Peak CPS signal ± SD of pH-MBs under neutral conditions (pH 7.4) and after acidification (pH 5) ($n = 3$), ****$p < 0.0001$. Error bars represent standard deviation. (E) Activation reversibility study of pH-MBs when cycling between pH 5.0 and 7.4 after initial activation.

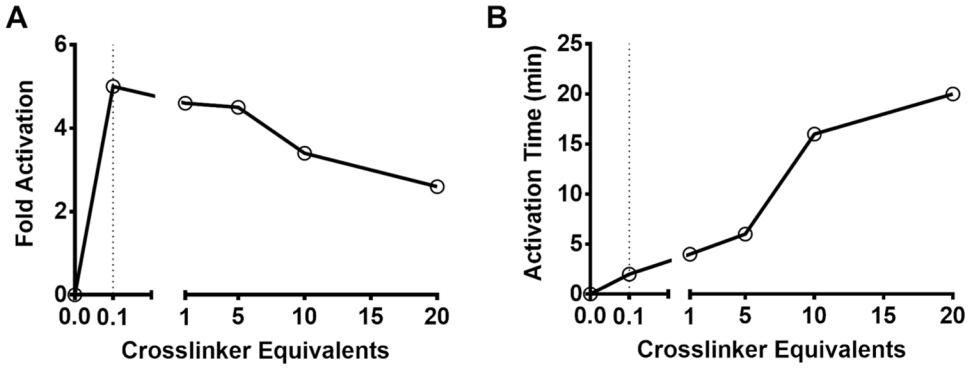

Figure 6.

Activation trends of pH-MBs. (A) CPS intensity increase (fold) of pH-MBs versus varying cross-linker equivalents. (B) Time to peak (min) versus varying cross-linker equivalents.